






RESEARCH ARTICLE

Battery pack technological considerations for hybrid-electric regional aircraft feasibility

A. Spinelli¹, G.P. Krupa¹, T. Kipouros¹, P. Laskaridis¹ and B. Berseneff²

¹Faculty of Engineering and Applied Sciences, Cranfield University, Cranfield, UK

²CEA, Université Grenoble Alpes, Grenoble, France

Corresponding author: A. Spinelli; Email: andrea.spinelli@cranfield.ac.uk

Received: 14 June 2024; **Revised:** 7 November 2024; **Accepted:** 12 November 2024

Keywords: hybrid-electric aircraft; sustainable aviation; aircraft design; battery technology; energy management system

Abstract

This paper presents a study of the effects of the durability and level of energy storage technology on energy management strategies and the performance of hybrid electric turboprops. The results highlight the key role of battery energy density on the durability of the battery pack and the viability of the concept of hybrid electric aircraft. Additionally, the trade-off between zero-day environmental compatibility and battery lifetime is identified, caused by the size of the pack. The effective energy density would decrease with the aging of the cells, leaving a significant inert mass and increasing fuel consumption. Optimal energy management strategies are suggested in light of this new information. Higher specific energy of the pack would mitigate this aspect, along with a reduction in fuel consumption and NO_x emissions. Indeed, the improvement of environmental compatibility was found to be nonlinear with a positive rate, suggesting high returns in investing in great improvements in energy density over a gradual increase. This result relates to the results of the statistical technological forecast presented in this study, which, without an increase in funding, predicts the availability of the specific energy required to match the fuel-only baseline in the 2040–2050 decade.

Nomenclature

C_r	a	battery cell equivalent capacitance (Farad)
DOH		degree of hybridisation
DOD		battery depth of discharge
E_{cell}		energy capacity of the cell (Ah)
$e_{battery}$		energy density of the battery pack (Wh/kg)
$E_{mission}$		total charge required to fly the mission (Ah)
F_{flow}		gas turbine fuel flow (kg/s)
h		degree of hybridisation (as defined in the EMS)
k		pack-to-cell mass ratio
I_{cell}		current in the cell (A)
M_{TO}		take-off mass (kg)
M_f		fuel mass (kg)
M_b		battery pack mass (kg)
N_{series}		number of cells in series per bar
$N_{modules}$		number of modules in parallel in the pack
P_B		power required by the battery pack
P_{GT}		power required by the gas turbine
P_{sat}		minimum probability to satisfy a constraint
R_0		cell internal resistance (Ohm)
R_t		RC transient resistance (Ohm)
U_{cell}		cell capacitance voltage (V)

V_c	RC transient resistance (Ohm)
V_{OC}	cell open-circuit voltage (V)
V_{sys}	system nominal voltage (V)

Greek symbol

Δ_{DOH}	slope of the linear degree of hybridisation function
η_E	efficiency of the electrical powertrain (propeller-to-battery)
η_{GT}	efficiency of the thermal powertrain (propeller-to-gas turbine)
μ_{DOH}	average degree of hybridisation of a linear function

1.0 Introduction

Since the beginning of the twentieth century, aeronautical research has been focused on reducing its global footprint on the environment by reducing emissions. Recent advances in battery technology and electrified ground vehicles have spurred research and investigation into the electrification of aircraft propulsion. One domain of research consists of introducing electric power in synergy with internal combustion engines in a hybrid propulsion system. The general idea is to maintain the internal combustion engines in the ideal operating condition when flying in high power conditions [1]. Finding the correct amount of electric power to achieve this ideal condition is the objective of the Energy Management System (EMS).

Both the system parameters and the flight path contribute to the identification of the optimal EMS. Many authors in the literature have explored the interaction between the flightpath and EMS, both in a local optimisation and global optimisation fashion with a fixed hybrid electric (HE) propulsion system configuration [2–4]. On the other hand, there has been little published work on the interaction between the hybrid propulsion system and the optimal EMS for a design mission, such as the role of the EMS in battery aging. Additionally, most authors assume a value of battery-specific energy without estimating the likelihood it will be available in the selected entry-into-service year. Given that this parameter is critical in the feasibility of HE aircraft, and currently there is a wide gap between the required technology and the state-of-the-art, it is worth investigating a plausible timeframe of HE adoption starting from past and future trends in cell energy density.

This paper attempts to address these two points through the application of a set-based design space exploration framework, previously published by the authors [5]. Section 2 covers a brief overview of the published literature related to the work presented in this study. Section 3 briefly describes the design space framework, the technological estimation method, and all the details of the adopted aircraft model. Details of the test case are presented in Section 4, while results are discussed in detail in Section 5. It first presents a thorough analysis of the effects of battery energy density, aging, and EMS on the performance of the aircraft, alongside a suggested definition of the EMS. Subsequently, the selected values of specific energy are evaluated in light of their plausible year of technological availability, according to the statistical analysis. Section 6 summarises the learned aspects with suggestions for future work.

2.0 Review of related work

The electrification of aircraft propulsion has been proposed as a potential solution to reduce the impact of aviation on the environment and its contribution to climate change. Hybrid-electric (HE) propulsion is one of the technical solutions investigated to achieve this goal. Two complementary sources of energy are used in synergy, low-efficiency but high-density fuel with high-efficiency and low-density electricity. These can be arranged as parallel, i.e. both provide direct power to the propeller shaft, or in series, where the gas turbine is linked to the propeller through a generator. Although the parallel configuration is simpler to implement, the mechanical link would alter the operating condition of the gas turbine,

Table 1. Battery pack energy density values adopted in literature studies of hybrid-electric regional aircraft

EIS (yr)	e_{pack} (Wh/kg)				
	250–350	500–600	750	1,000	1,500
2025–2030	[7, 19, 20]				
2030–2040	[15, 21, 22]	[9, 11, 13]	[9, 11, 12]	[9, 12, 14]	[12]
2040–2050		[5, 21]	[21]		
Not specified		[20, 23]			

reducing its surge margin [6]. On the contrary, the series layout decouples the gas turbine from the propulsors, enabling exotic configurations such as boundary layer ingestion (BLI). However, the lower efficiency of the power chain and its weight can offset the performance benefits of maintaining the gas turbine in its ideal operating condition [7]. The proposals for HE aircraft range from general aviation [8], regional and commuter turboprops [9], to 180-passenger single aisle airliners [10]. Nonetheless, the practical adoption of HE propulsion is limited by the technological development of the battery pack.

Table 1 summarises the adopted pack energy density value for several published works on regional hybrid-electric turboprop aircraft. These studies often include an expected entry into service (EIS) year that ranges from 2030 to 2040, with the most widely adopted figure being 2035 [11–15]. The value adopted for the e_{pack} ranges from 500 to 1,500Wh/kg. Both the specific energy and the short time frame are very optimistic. The current state of the art for cell technology is reported at 260Wh/kg [16], which is effectively eroded by the packaging material and accessories of the battery pack by at least a factor of 33% [17]. Furthermore, no provisions are present in the FAR-25/CS-25 regulations for HE aircraft. Therefore, a 10-year development and certification timeline could be too optimistic, as regulatory bodies would require more time to draft the relevant regulations [18].

Another point of note is the energy management strategy (EMS) adopted in these studies. Most adopt one constant value of the degree of hybridisation (DOH) either for the entire mission [9, 12], or different constant DOHs for each mission segment [11, 19]. Hoelzen et al. [14] proposed a different approach to EMS, where the electrical energy would be supplied to boost a downsized gas turbine. This strategy is named ‘power shaving’ and has been adopted to boost cruise in studies published by Spierling and Lents [15] and Cinar et al. [22]. Its advantage is in keeping the gas turbine in its ideal range and in sizing the battery pack only for boosting energy, rather than for the entire mission. Therefore, the weight penalty due to the low specific energy of the cells is reduced. Decerio and Hall [20] also suggested to use electric power to boost climb. In a previously published study, the authors suggested that climb and cruise were the mission phases that provided the main contribution to the reduction of fuel consumption and NO_x emissions when hybridised [5].

Only two of the studies reported in Table 1 distinguish between the energy density of the cells and the energy density of the packaged battery [15, 22]. Most of the publications adopted a conceptual level of fidelity and focused on the reduction of CO₂, fuel consumption and noise of the hybrid-electric propulsion system. Hence, the detail of the battery pack behaviour was sacrificed for computational speed, especially when comparing multiple configurations [7, 11, 13, 19]. As a consequence, none of these studies takes into account the effects of battery pack aging on system performance.

In a real-world application, HE aircraft should be designed to guarantee its reduction in fuel consumption and emissions for a reasonable operating time, to justify its development and acquisition cost. Therefore, capturing the effects of aging in a conceptual design stage is fundamental. Clarke and Alonso developed a model that includes both aging effects and thermal management [24]. When applied to an all-electric commuter aircraft, the battery capacity would drop by 25% after one year of operation. Similarly, when investigating an electric urban air mobility vehicle [25], the reduction was as high as 45%. This dramatic reduction in energy storage propagates in a reduced range and/or payload. In an HE aircraft, instead, it increases fuel consumption to compensate for lost energy [26].

The complexity of the design of an HE aircraft is caused by the uncertainty in its technological requirements and the knowledge about the behaviour of the system. Recent frameworks applied in HE designs focus more on simulation and optimisation, without evaluating the impact of technological uncertainty [11, 27, 28]. The reason is due to the difficulty in predicting the value interval, as no hybrid electric aircraft has yet reached production. This gap is highlighted in recent state-of-the-art reviews of HE aircraft [29, 30] and is part of NASA Vision2040 plan [31].

Di Bianchi et al. [32] developed a framework employing probability distribution on technology parameters and propagating them in an optimisation problem. The output data is processed and presented with the use of visual analytics tools to interactively explore the design space and build a portfolio of options. Guenov et al. [33] adopted probability theory as a method to quantify the probability that a requirement is satisfied. Margins would be adopted to increase the robustness of the requirement, lowering its uncertainty. Wahler et al. [34] presented a methodology to estimate the probability that a conceptual design that incorporates innovative technologies will be available in the future. The HE aircraft design is framed as an optimisation problem to achieve the highest range possible under credibility constraints, the probability that a technology is achievable by the specified EIS year. These are quantified using probability density functions on relevant quantities such as battery energy density or drag reduction from natural laminar flow aerofoils.

3.0 Methodology

The methodology section is divided in two main parts: the first one describes the numerical design methods adopted in this article while the second describes the modelling of the system under design. Given the large number of possible combinations of input parameters, a novel design space exploration framework is used to reduce the number of designs to evaluate with the multi-disciplinary optimiser (Section 3.1). The main technological assumption, the battery energy density, is also evaluated for its credibility using the probabilistic method presented in Section 3.2. Details for the design model are then presented, with discussion of the aircraft performance model in Section 3.3 and the battery modelling in Sections 3.4 and 3.5. Finally, the mission analysis algorithm is presented in Section 3.6 with the description of the energy management strategy explored and the design mission in Section 3.7.

3.1 Design space exploration methodology

The results presented in this article has been generated by adopting a design space exploration framework developed by the authors, known as PDOPT [35]. This methodology has been developed to explore design problems featuring a high variance in the design space: many input parameters with wide ranges. Running a population-based optimiser in the whole design space would be costly, especially if most of it is not feasible. The problem explored in this study, as described in Section 4, presents a high input parameter variability: the total number of combinations to be evaluated are 1,536. PDOPT was demonstrated to successfully reduce the computational cost by 80% in problems with high variability [5, 36].

While not the focus of this article, the core principles of the framework are reported. For further details, the reader should consult the previously published literature [5, 35]. Figure 1 presents the process for analysing a given design space and producing feasible design points. The central idea is reducing the number of unfeasible alternatives by estimating the probability of satisfying the constraints of the multi-disciplinary optimisation problem underlying the design task. Indeed, within PDOPT requirements are cast as a constraint over an output quantity calculated by the design model. This probability is used to decide if the evaluated portion of the design space is worth further exploring with a local optimisation algorithm or not. This procedure is akin to reducing the uncertainty of requirements mapping onto the design space: the range of possible inputs that the designer can choose is reduced, increasing the confidence in finding the suitable designs. Additionally, the constraints are mapped without any assumptions on the user: the information relating input parameters to quantities of interest is extracted from the design model directly, increasing the robustness of the approach.

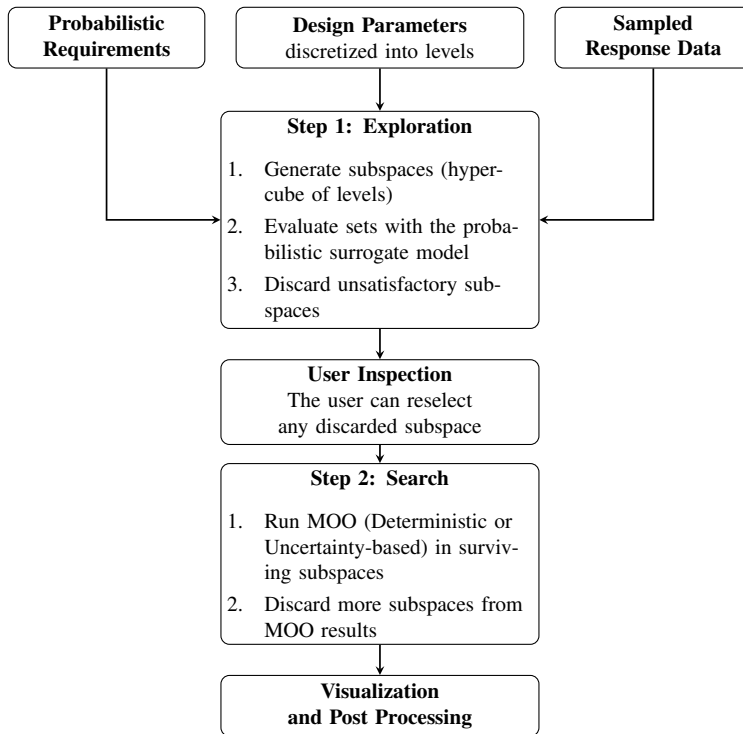


Figure 1. Methodology flowchart.

Within PDOPT this elimination process is called ‘Exploration Phase’ and incorporates one the core principles of Set-Based Design [37]: that is focusing on eliminating unfeasible portions of the design space, rather than selecting the most feasible in the early stages of the design process. Adopting this approach has been demonstrated to reduce rework caused by design mistakes [38] and increase design robustness [39, 40]. Each design space portion is called ‘set’, and is evaluated by sampling with a Gaussian process trained on the design model data. The calculated probability is compared to the threshold value P_{sat} (satisfaction probability) to decide if it is eliminated or not. Using a probabilistic approach allows to handle those portions of the design space that are crossed by the boundary of the requirement, hence avoiding eliminating possible feasible solutions.

The subsequent phase, the ‘Search Phase’, recovers the individual design points from the surviving sets by running optimisation problems bounded by the set limits. This enables to refine and verify the constraints locally. The result is a dataset of multiple alternative design points that satisfy the constraints. The Pareto front that is obtained may be contained within a set, however, maintaining the alternatives allows the designer to restrict the constraints or perform other analyses without requiring re-computation. This is the case of this study, as the goal is to understand the interaction between the aircraft propulsion system, the battery pack, and the energy management strategy without any assumption of the best design. Results are processed using multi-axis techniques such as Parallel coordinates plots [41], which enable to highlight relationships in combination with scatter plots.

3.2 Likelihood estimation of future battery technology

Since e_{pack} is a critical technological parameter for the feasibility of the proposed HE designs, a method is adopted to estimate the probability of availability. Data have been extracted from the Battery 2030+ Roadmap report [42] from the year 2010 onward, including target values of energy density up to the year

2030. The dataset includes 35 points from different sources and projects around the world for Lithium-based batteries. The procedure consists of constructing a linear regression model using Ordinary Least Squares (OLS) of the cell energy density data. Equations (1) are used to estimate the coefficients of the linear model $y_{e_{cell}} = b_1 \cdot x_{year} + b_0$ and the regression variance σ .

$$\begin{aligned} \bar{x} &= \frac{1}{n} \sum_{i=0}^n x_i \\ \bar{y} &= \frac{1}{n} \sum_{i=0}^n y_i \\ S_{xx} &= \sum_{i=0}^n x_i^2 - \frac{1}{n} \left(\sum_{i=0}^n x_i \right)^2 \\ S_{xy} &= \sum_{i=0}^n y_i x_i - \frac{1}{n} \left(\sum_{i=0}^n y_i \sum_{i=0}^n x_i \right) \\ b_1 &= \frac{S_{xy}}{S_{xx}} \\ b_0 &= \bar{y} - b_1 \cdot \bar{x} \\ \sigma &= \sqrt{\sum_{i=0}^n (y_i - \bar{y})^2 - b_1 \cdot S_{xy}} \end{aligned} \tag{1}$$

Once the coefficients are found, it is possible to predict the mean and variance of the cell energy density for a specific year X_{year} using Equations (2). These statistical parameters describe a Gaussian distribution centred in $\mu_{e_{cell}}$ and standard deviation $\sigma_{e_{cell}}$.

$$\begin{aligned} \mu_{e_{cell}}(X_{year}) &= b_1 \cdot X_{year} + b_0 \\ \sigma_{e_{cell}}(X_{year}) &= \sqrt{\sigma^2 \left[1 + \frac{1}{n} + \frac{X_{year} - \bar{x}}{S_{xx}} \right]} \end{aligned} \tag{2}$$

To predict the pack energy density, the relation between e_{pack} and e_{cell} must be found through the pack-to-cell mass ratio k , which is defined as follows:

$$k = \frac{M_{pack}}{N_{cells} \cdot M_{cell}} \tag{3}$$

where N_{cells} is the number of cells in the pack, M_{cell} the mass of a single cell, and M_{pack} the mass of the entire battery pack. By replacing the definition of energy density $e = E/M$ and remembering that the pack electric energy is equal to $E_{pack} = N_{cells} \cdot E_{cell}$, the following scaling equation is obtained with a few algebraic steps:

$$e_{pack} = \frac{e_{cell}}{k} \tag{4}$$

which states that the effective energy density of the pack is lower than that of the cell one. Finally, it is possible to estimate the probability that a specific pack energy density is available in a year X_{year} using:

$$P_{e_{pack}}(X_{year}) = 1 - \Phi \left(\frac{k \cdot e_{pack} - \mu_{e_{cell}}(X_{year})}{\sigma_{e_{cell}}(X_{year})} \right) \tag{5}$$

where Φ is the Gaussian cumulative distribution function. Two scenarios were developed from the same data set. The first one, labeled ‘conservative’, assumes a linear improvement of the cell energy density, hence no change in the rate of technological development. In contrast, the second scenario, named

Table 2. Aircraft properties

Maximum take-off mass	23,000kg	Payload mass	5,000kg
Operating empty mass	11,550kg	Gearbox efficiency	0.99
L/D Climbout	10.5	Propeller efficiency (Take-Off)	0.64
L/D Climb/Descent	16	Propeller efficiency (Climb)	0.73
L/D Cruise	14.5	Propeller efficiency (Cruise)	0.86
L/D Final	7.5	Propeller efficiency (Other)	0.8

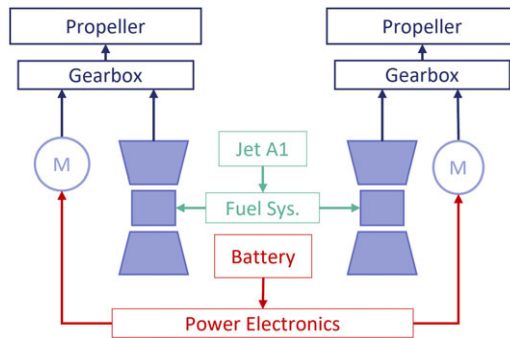


Figure 2. Propulsion system architecture.

‘optimistic’, hypothesises the increment of R&D funding towards energy storage, hence it features an exponential regression model. The same Equations (1) and (2) can be used using the following regression model:

$$\log (y_{e_{cell}}) = b_1 \cdot \log (x_{year}) + b_0 \tag{6}$$

In addition, two pack-to-cell ratios are used in both scenarios to estimate the impact of battery packaging technology on the availability year. The adopted values are 1.5, commonly used in the published literature for the design of electrified aircrafts [43], and 2.0 as a more conservative alternative. The reader should be aware this parameter is heavily influenced by the safety requirements of the battery pack, the cooling system and the onboard battery management system. Hence, it is difficult to estimate in a conceptual design scenario: adopting two extreme values allow to cover the possible outcomes of this uncertain parameter.

3.3 Aircraft and propulsion model

The selected aircraft is a 50-seater turboprop obtained by retrofitting an ATR-72, where part of the payload mass has been replaced by the mass of the battery pack. Mass and aerodynamic data have been extracted from information available on the ATR 72-600 [44, 45]. These are presented in Table 2. The operating empty mass (OEM) figure is kept constant as it is assumed that the mass of the electrical equipment that is not the battery pack has a marginal contribution to the total take-off mass increment. Therefore, it has been ignored since this high-level study does not consider the sizing of these components. Furthermore, a major assumption is that the OEM does not change with the battery pack mass, and structural resizing is neglected, therefore, the maximum take-off weight of the reference ATR-72 is imposed as a constraint.

The propulsion system is a mechanically integrated parallel hybrid propulsion unit, whose power is provided by a gas turbine and an electric motor, as shown in Fig. 2.

Table 3. Electric propulsion system parameters

Electric motor efficiency	0.98
Power electronics efficiency	0.985
Cable distribution efficiency (circuit breakers)	0.996
Packaging factor (pack-to-cell mass ratio)	1.5
Cell total capacity (Ah)	7
Cell nominal voltage (V)	3.7
Cell mass (kg)	0.0518

The gas turbine is a thermodynamically equivalent model of the Pratt & Whitney Canada PW127 engine, whose performance data have been generated using the in-house code TURBOMATCH [46, 47]. It is assumed that the electric propulsion component is introduced as a retrofit to the aircraft; hence the baseline gas turbine is not resized for hybridisation. Constant propeller efficiency has been assumed for different mission phases. The NO_x emissions model is based on the Boeing FuelFlow2 method [48], which is a simplified P3T3 method useful when manufacturer data is not available. The data required to model the turboprop emission indice $E_{I_{NO_x}}$ was collected from Filippone and Bojdo [49].

Electric motors, power electronics, and cabling are modeled with a single constant efficiency parameter, the values of which have been adopted from Ref. (50). The battery pack is modeled with a Thevenin equivalent circuit, as explained in Section 3.4. The TMS is assumed to keep the battery temperature at 25 °C. A TMS will be designed and modeled, and its dynamic off-design performance impact on the battery temperature and its operation will be investigated in the final paper.

3.4 Battery model

To capture in detail the efficiency of the battery pack and its behaviour when subjected to different energy management strategies, a Thevenin equivalent circuit model (Fig. 3) was developed [51]. Equations (7) describe the behaviour of a single battery cell. Reference (52) provided the equations for the behaviour of the lumped components V_{OC} , R_0 , C_t , R_t under different values of depth of discharge DOD , while the properties of the cell are presented in Table 3. The cell mass is scaled to match the selected battery pack energy density, without changing the capacity of the cell itself, and thus not invalidating the ECM model. The pack-to-cell mass ratio is 1.5, taken from the battery model of the NASA X-57 Maxwell [43]. However, this value is optimistic, as the safety and certification requirements would increase the insert mass of the pack [17].

$$\frac{dV_C}{dt} = \frac{I_{cell}(t)}{C_t} - \frac{V_C(t)}{R_t C_t}$$

$$\frac{dDOD}{dt} = \frac{I_{cell}(t)}{E_{cell}} \quad (7)$$

$$U_{cell} = V_{OC} - V_t - I_{cell} R_0$$

$$P_B = U_{cell} I_{cell} (N_{series} \times N_{modules})$$

The power provided to the cell is calculated by dividing the required battery power at the pack terminals. The pack is composed of groups of cells in series called modules, which are arranged in parallel to each other to meet the required capacity. The battery pack sizing procedure is as follows:

1. Calculate the number of cells in series for each module to meet the nominal system voltage:

$$N_{series} = \frac{V_{sys}}{V_{cell}}$$

2. Increment the energy required to fly the mission by a guessed factor m : $E_{total} = m \cdot E_{mission}$

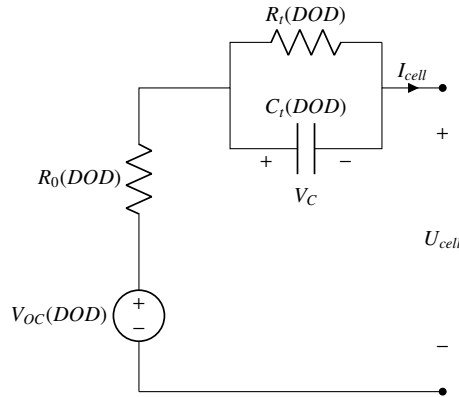


Figure 3. Thevenin electric model for a battery cell.

3. Calculate the number of modules to meet the required energy: $N_{modules} = \frac{E_{total}}{E_{cell}}$
4. Simulate the cell discharge by solving the ODE system in Equation (7) after dividing the pack power by the total number of cells $P_{cell} = \frac{P_B}{N_{series}N_{modules}}$
5. Repeat steps 2–4 by changing m , until the pack depth of discharge matches the target of 80%.
6. Calculate the total mass of the pack by multiplying the number of cells by the cell mass. This value is then increased by the pack-to-cell mass factor k to account for the mass overheads caused by the wiring and casing.

With the battery pack properly sized, the circuit model is run to evaluate the efficiency of the battery pack and its discharge characteristics. In this model we ignore the C-rate of the cell, which may further reduce the maximum current between each module. This may require more modules in parallel than the ones required by the required capacity in certain situations. Since this information is dependant on the brand and type of the battery, it has been neglected for simplicity.

3.5 Battery ageing model

The holistic ageing model developed in Ref. (53) was adopted to model the loss of energy and capacity of the cell and the growth of its internal resistance, as it is put into operational use. Equations (8) are used to update the equivalent circuit model parameters (cell capacity, capacitance and resistance) with the contributions from calendar ageing (parameter α) and cycle ageing (parameter β). The first is proportional to the number of days of use t , while the second is proportional to the total lifetime charge Q that has passed through the cell.

$$C = C_0 \cdot \left(1 - \alpha_c \cdot t^{0.75} - \beta_c \cdot \sqrt{Q} \right) \tag{8}$$

$$R = R_0 \cdot \left(1 + \alpha_r \cdot t^{0.75} + \beta_r \cdot Q \right)$$

The update procedure is performed after one iteration of the ageing simulation, where the results of the equivalent circuit dynamics of 7 (current, voltage, and depth of discharge) are used to calculate the parameters of the ageing model. Specifically, calendar ageing is affected by storage temperature T and storage voltage V (Equation 9), while cycle ageing is proportional to the root mean square voltage V_{rms} and the difference in depth of discharge of the operating cycle ΔDOD (Equation 10). For the purpose of this study, storage temperature is kept constant as it is assumed that the thermal management system

maintains it in the ideal range.

$$\alpha_c = (7.543 \cdot V - 23.75) \cdot 10^6 \cdot e^{-\frac{6976}{V}} \quad (9)$$

$$\alpha_r = (5.270 \cdot V - 16.32) \cdot 10^5 \cdot e^{-\frac{5986}{V}}$$

$$\beta_c = 7.348 \cdot 10^{-3} \cdot (V_{rms} - 3.667)^2 + 7.600 \cdot 10^{-4} + 4.081 \cdot 10^{-3} \cdot \Delta DOD \quad (10)$$

$$\beta_r = 2.153 \cdot 10^{-4} \cdot (V_{rms} - 3.725)^2 + 1.521 \cdot 10^{-5} + 2.798 \cdot 10^{-4} \cdot \Delta DOD$$

The battery pack ageing simulation is performed by running the mission analysis and updating the cell parameters after a certain amount of time has passed. This study evaluates the battery pack performance after one year of operations, assuming two flights per day, seven days per week. A five-day time step was selected as an adequate trade-off between computational cost and error.

3.6 Mission analysis method

Figure 4 presents the procedure used to find the burned fuel mass and the mass of the battery pack for the specified mission. After an initial guess of the fuel mass M_f and the battery pack mass M_b , the take-off mass of the mission M_{TO} is calculated and updated iteratively until both the fuel and battery pack masses converge. Two nested loops are used, the innermost for M_f and the outermost for M_b .

The analysis is performed by splitting the entire mission into small parts and, calculating for each of them the power required to fly its phase, using the altitude h , velocity V , and climb rate V_z prescribed by the mission. This power is then divided between the two powertrains with the specified degree of hybridisation DOH , and chain efficiencies are applied to calculate the power required by the gas turbine P_{GT} and by the battery pack P_B . The burned fuel mass is calculated by multiplying the current fuel flow F_{flow} of the gas turbine by the elapsed time and summed over all the phases of the mission. Once the fuel mass is converged, the total charge is calculated and used to size the battery pack according to the procedure explained in 3.4. After the battery pack is sized, the degradation condition is evaluated. The procedure simulates one year of operational life, updating the energy capacity and internal resistance every five days. At each step, the original energy management DOH is scaled proportionally, without changing its topology, to avoid the battery going above the 80% depth of discharge. Since the capacity of the cells reduces as it ages, more fuel is required to carry out the same mission, therefore it is reasonable to adopt as a representative variable for battery aging the ratio between the original fuel consumption and the fuel consumption after one year of use (Equation 11).

$$r_{degr} = \frac{M_{fuel, 1 \text{ year use}}}{M_{fuel, fresh \text{ battery}}} \quad (11)$$

3.7 Design mission and energy management profile

The selected mission profile is shown in Fig. 5, which has been adopted by the FutPrint50 [54] project as a maximum range design mission, including a flight to an alternative airport to account for fuel reserves. The main flight stage is 432nm (800km) and the alternative stage is 51nm (95km) with a 30-minute holding pattern. The average climb rate is 996ft/min (5.059m/s), while the cruise speed is 268kt (137.78m/s).

It is assumed that the aircraft would have exhausted its energy reserves (fuel and batteries) at the end of the entire flight. Electric power use is restricted to the climb and cruise phases of the main portion of the mission. Since the focus of this study is in energy modelling, short flight segments such as take-off are ignored. However, in a real world scenario the take-off phase is important to size the maximum power of the electrical motor and gas turbine. Furthermore, using electrical power in this segment would reduce aerodrome noise, which is an important pollutant.

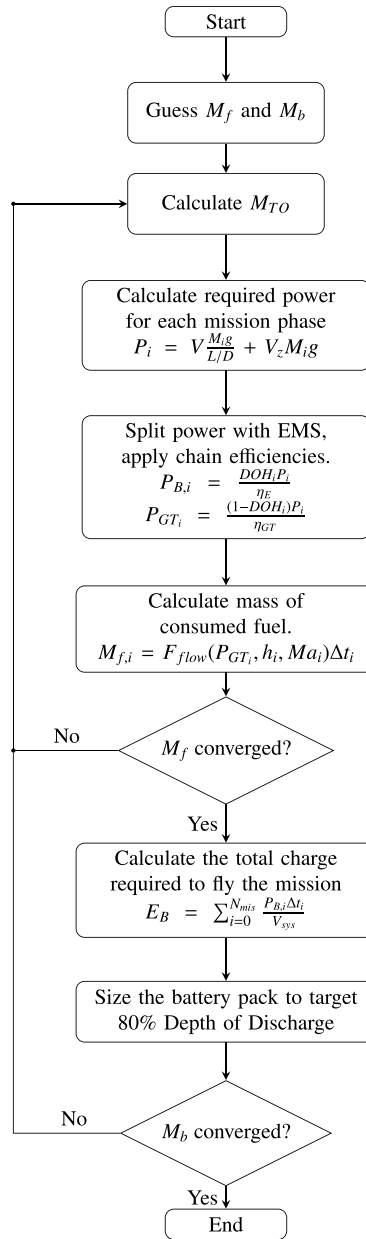


Figure 4. Mission analysis method flowchart.

Energy management strategies are defined as a continuous piecewise linear DOH function throughout the mission, with values ranging from 0 to 1 (Fig. 6), as detailed in Ref. (5). These parameters allow for a flexible definition of the shape of the EMS in each phase. In total, four parameters describe a complete energy management strategy for a full mission analysis.

4.0 Test case

The design space exploration test case is formulated as an optimisation problem, as shown in Equation (12). For this study, we consider linear energy management segments, applied to the climb and cruise

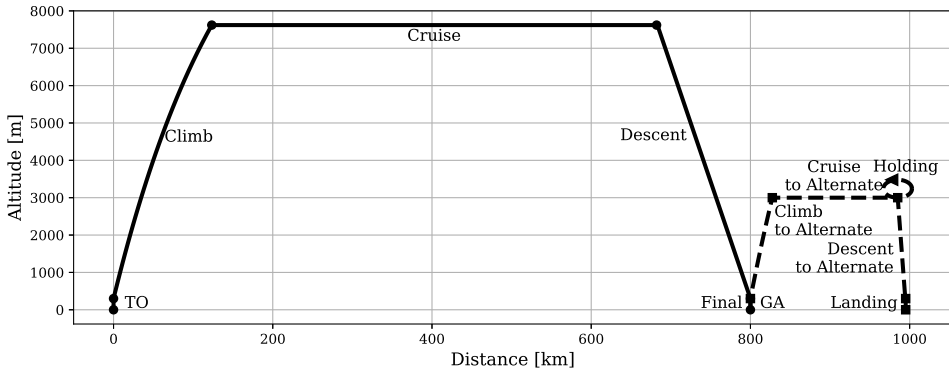


Figure 5. Mission profile.

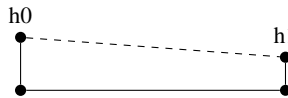


Figure 6. Linear energy management strategy adopted for this study.

phases, and the energy density of the battery pack. The input values for the PDOPT framework are presented in Table 4. Within the explored alternatives of pack energy density, the 750Wh/kg value was added as a highly futuristic technological scenario. The selected figures of merit are the total fuel burned during the mission M_f , the mass of the emitted NO_x , and the ratio of the mass of burned fuel after one year of operation to the original amount with a fresh battery pack.

$$\begin{aligned}
 &\text{given} && X = \{e_{battery}, h0_{cl}, h1_{cl}, h0_{cr}, h1_{cr}\} \\
 &\text{minimize}_X && M_{fuel}, M_{NO_x}, r_{degr} \\
 &\text{subject to} && M_{TO} \leq 23000 \text{ kg} (P_{sat} \geq 0.5)
 \end{aligned} \tag{12}$$

The last objective is to study the effects on system performance of aggressive hybridisation when the battery pack is fresh. While it is not directly a battery pack parameter, it is an indicator of how much the capacity of the cell has degraded over one year of operation. Indeed, to meet the same target 80% of DOD, the energy management system must use more power from the gas turbine powertrain, leading to higher fuel consumption and higher emissions. Within the simulation code, the battery pack is sized such that it would reach 80% DOD at the end of the mission, in other words it would be fully discharged after delivering all its electrical energy according to the EMS it is sized to.

The take-off mass M_{TO} is restricted to the maximum take-off mass of ATR-72, and introduced as a probabilistic constraint to the exploration step, with a minimum satisfaction probability P_{sat} of 50%. Areas of the design space that fall below this threshold are discarded and not considered for optimisation.

Results are compared to the baseline, which is the same ATR-72 model without electric propulsion and loaded with the same payload. The values of the baseline are presented in Table 5.

5.0 Results

Figure 7 presents the Pareto front solutions produced by the design space exploration framework. Three main results are clear from this graph. First, a high $e_{battery}$ produces higher values of r_{degr} overall. However, when comparing equal values of fuel burn reduction, the battery ages slower when the specific energy is higher (Fig. 7(a)). As will be discussed later, this is caused by the mass of the cells and not by cell aging

Table 4. Input parameters

Parameter		Values
Pack energy density (Wh/kg)	$e_{battery}$	[350,400,450,500,550,750]
Start Climb DOH	$h_{0_{cl}}$	(0,1) divided into 4 levels
End Climb DOH	$h_{1_{cl}}$	(0,1) divided into 4 levels
Start Cruise DOH	$h_{0_{cr}}$	(0,1) divided into 4 levels
End Cruise DOH	$h_{1_{cr}}$	(0,1) divided into 4 levels

Table 5. Baseline quantities

Take-off mass	17,792kg
Burned fuel	1,242kg
NO _x emission	8.59kg

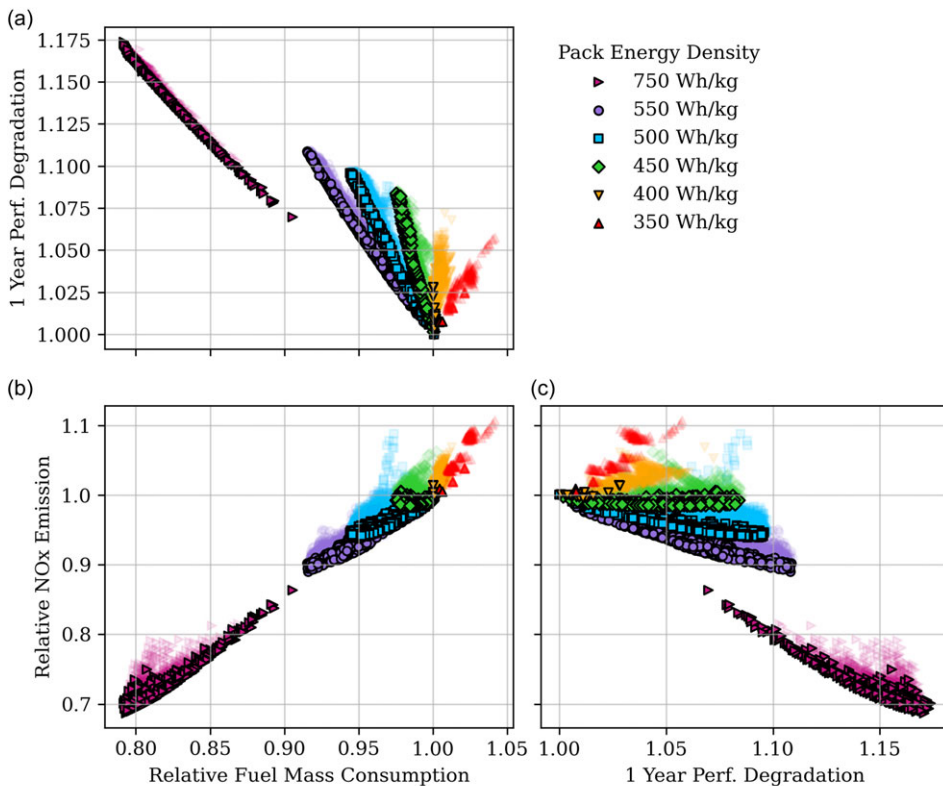


Figure 7. Pareto front of the three objectives with different battery pack energy densities.

(Fig. 10). With more energy per unit of mass, fewer cells are required to achieve the same reduction in fuel consumption. The airplane is less heavy; hence, when the capacity fades over time, the dead weight of the batteries has a smaller impact on fuel consumption. Instead, when all the mass available for batteries is used, the rate of degradation is higher because of the higher extra dead weight. It can be noted here that the rate of improvement of both fuel consumption and NO_x emissions increment non-linearly with $e_{battery}$. This aspect will be discussed in detail in Section 5.6 with its technological implications.

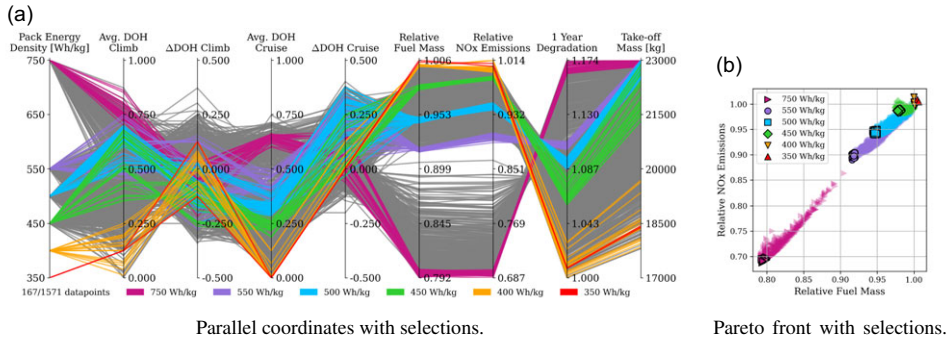


Figure 8. Effects of battery energy density on the energy management strategies.

Secondly, the rate of degradation and the other two objectives compete, most evidently, with the reduction of fuel consumption. This trade-off is important for airline operators, where the cost of fuel and the cost of battery maintenance would compete.

Finally, the results indicate that the pack energy density should be greater than 400Wh/kg to reduce the emissions and fuel consumption above the baseline (Fig. 7(b)). This sets a technological requirement of a minimum 600Wh/kg energy density for individual cells, which would be available no earlier than the year 2040 according to the prediction in Section 5.6.

While not the focus of this study, the results also agree with previously published work by the authors [5], where the hybridisation of the climb segment affects mainly the NOx emissions (as a high power mission phase), where CO2 emissions are mainly affected by the hybridisation of the cruise segment (the longest in the flight). This study did not include effects of the battery energy density nor the degradation of the cells, which the present work seeks to extend. More details can be found in the published literature [5].

The following subsections explore the data in detail, analysing the interaction between $e_{battery}$, r_{degr} , EMS, and battery life alongside the performance of the aircraft compared to the baseline.

5.1 Effects of $e_{battery}$ on energy management strategies

Figure 8 presents the resulting optimal energy management strategies for each level of battery energy density. Since the strategies are all linear segments, the input variables have been decomposed into an average value, the midpoint of the segment, and a discrepancy, the slope of the segment, as shown in Equation (13).

$$\begin{cases} \mu_{DOH} = \frac{h_1 + h_0}{2} \\ \Delta DOH = \frac{h_1 - h_0}{2} \end{cases} \quad (13)$$

Higher values of energy density allow for higher values of average DOH , both in climb and cruise. More flight power can be provided by the electrical source at the same maximum take-off mass limit. The climb segment is more hybridised than the cruise segment. Regarding the slope of the segments, the cruise phase presents a positive slope directly correlated with the energy density. However, the climb segment presents a negative slope with some exceptions, mainly when $e_{battery}$ is 550Wh/kg. In conclusion, more specific energy in the battery pack enables more hybridisation and more flexibility in the slope of the segments, because it is possible to store more electrical power onboard for the same amount of maximum take-off mass.

5.2 Effects of r_{degr} on energy management strategies

Figure 9 presents for three different levels of battery energy density the effect of the degradation parameter r_{degr} over the other variables. Battery life was calculated as the number of days after which the electrified aircraft matches the fuel consumption of the baseline conventional aircraft (see Fig. 10(a)). It is correlated with r_{degr} , where the battery lasts the longest with low degradation EMS. All three technological scenarios feature similar correlations between r_{degr} and the average values of DOH : the higher the electrical power demand, the faster the cell degradation. On the other hand, ΔDOH is concentrated around zero when r_{degr} is the lowest. It spreads without a specific trend at values of high degradation. It can be concluded that the average electrical power requirement drives the degradation of the cell, rather than the specific value over time.

5.3 Effects of $e_{battery}$ on r_{degr} and battery life

Eight specific points, two per $e_{battery}$ value, were selected for analysing the history of battery degradation over one year of operation. Each pair consists of designs with the lowest fuel consumption at zero days and the longest battery life, as defined in the previous Section 5.2. Figure 10 presents these results on two scales: fuel consumption relative to the conventional baseline and relative to the zero-day condition. The original three values of $e_{battery}$ from Ref. (55) were simulated for a year, as their battery life was less than 365 days. On the contrary, the additional scenario of a battery with 750Wh/kg was simulated until reaching the end-of-life condition.

As shown in Fig. 10(a) the battery lifetime is longer with higher $e_{battery}$ and, respectively, the gap from the lowest degradation to the highest is larger for each case. At the most extreme value of 750Wh/kg, the lifetime is above 1,000 days. On the contrary, Fig. 10(b) shows that r_{degr} grows faster when $e_{battery}$ is greater and the degradation is high; the opposite is true when the degradation is low. This relative behaviour is present also with the battery pack of 750Wh/kg, however, both curves are shifted towards higher growth of relative fuel consumption increase. The cause is the more intense usage of electrical energy due to the high energy density. When the pack ages and its effective energy density goes down, fuel consumption grows faster to compensate for the lost electrical energy. Nonetheless, the large margin in energy density allows the propulsion system to improve over the baseline for a much longer time (see Fig. 10(a)).

Despite the differences between the eight scenarios, the actual degradation of the cell (capacity depletion and growth of internal resistance) is identical (Fig. 10(c) and (d)). Indeed, the parameters that would affect cell degradation, such as the temperature, initial state of charge, and depth of discharge, are identical for all the cases. This would change if partially recharging the airplane after one flight is introduced in the analysis, a scenario that has been suggested by the authors for regional aircraft operations [56]. More flights could be carried out per day, at the cost of using the battery from a partial state of charge, accelerating the aging of the cells.

Comparing the geometry of the battery packs of these six cases (Table 6) shows that the number of cell modules is correlated with the parameter r_{degr} of Fig. 10(b): the higher this quantity, the faster the rate of degradation. While each cell ages at the same rate, the airplane is carrying more weight, and therefore, with less electrical power compensating for the inefficiency of the extra weight, the fuel consumption grows faster as the battery ages. In summary, the effective specific energy of the pack decreases with cell aging, eroding the benefits calculated on day zero, with a leveraging effect caused by the size of the battery pack. Therefore, more specific energy from the start enables the battery to last longer before servicing, as demonstrated by the 750Wh/kg battery pack case.

5.4 Effects of $e_{battery}$ on aircraft performance

Figure 11 presents the percentile change in fuel consumption, energy consumption and take-off mass relative to the baseline. It contains three selections of the Pareto front for each level of battery pack technology. The values refer to the day-zero condition.

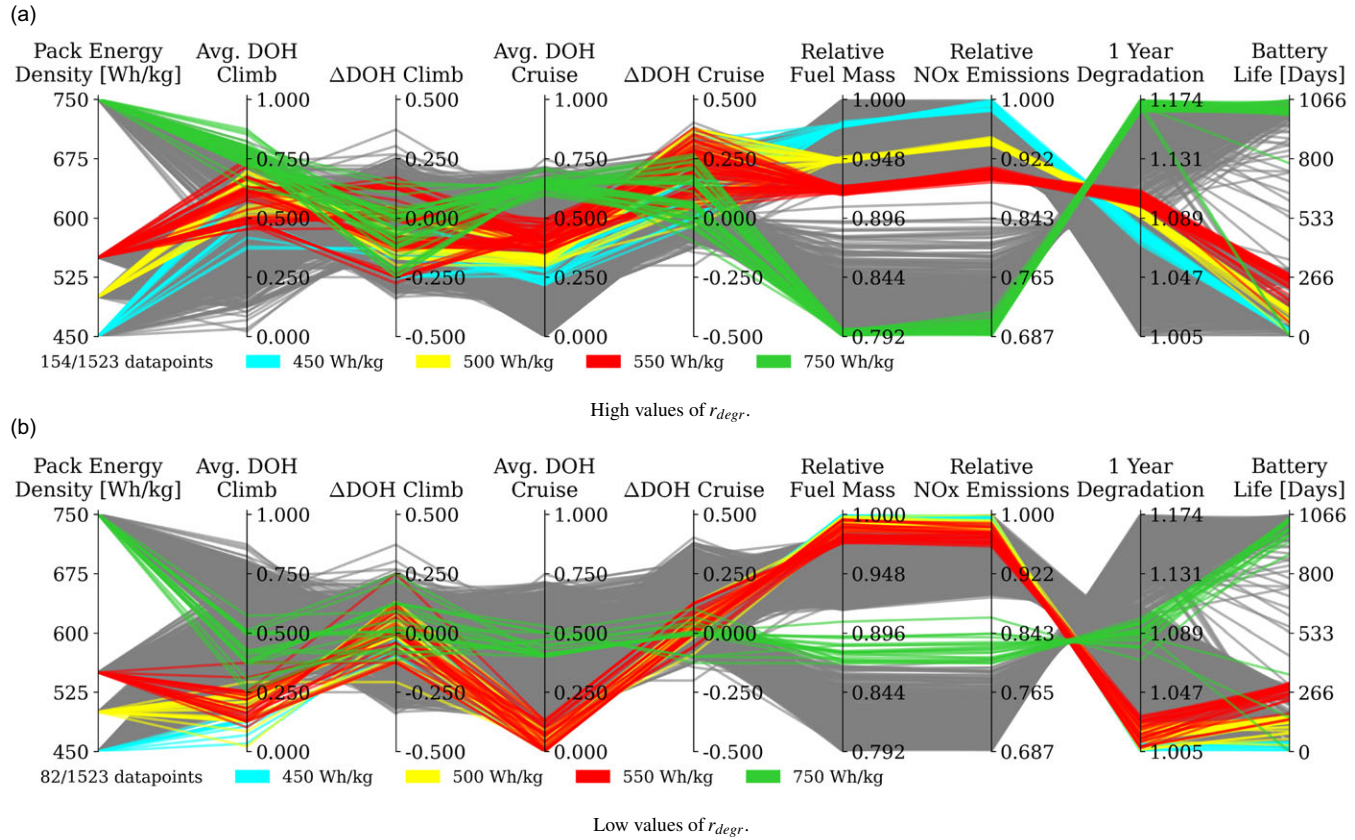


Figure 9. Effects of degradation on the energy management strategies.

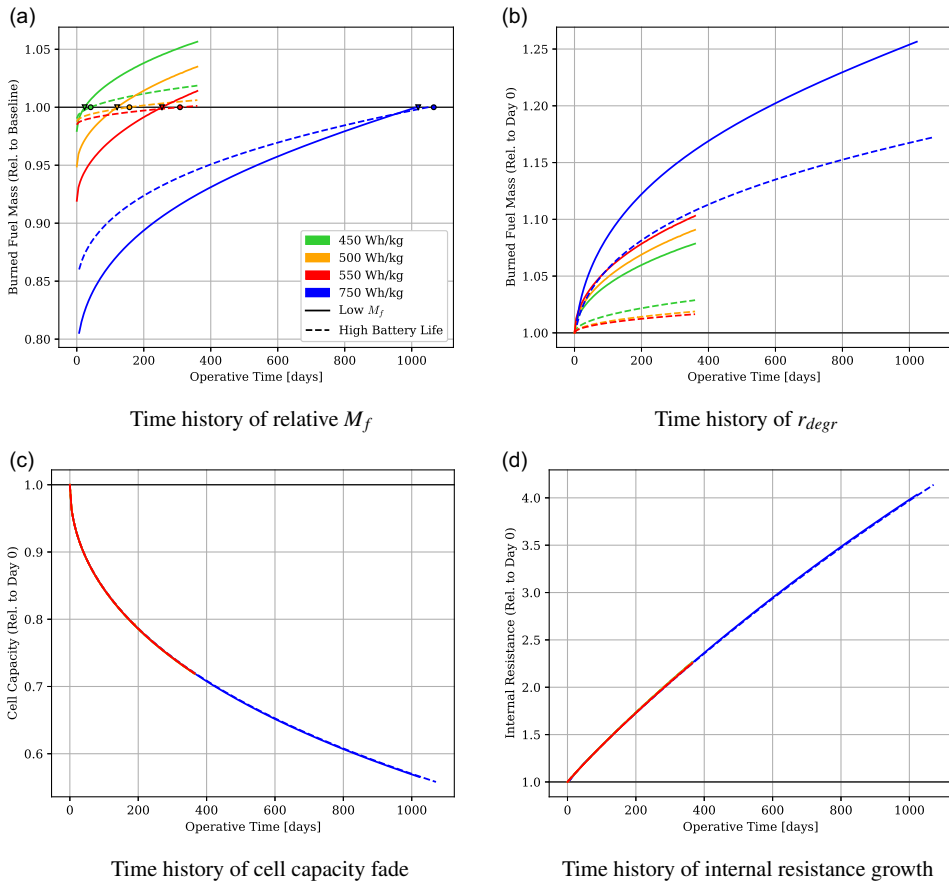


Figure 10. Degradation histories of extreme points for each $e_{battery}$ case.

All investigated cases are less efficient than the baseline, requiring more energy to fly the same mission. The specific energy of the fuel is at least 20 times higher than that of the batteries, increasing the take-off mass when trading one source for the other. Hence, the heavier airplane requires more energy to fly, despite the lower fuel consumption. When the take-off mass is constrained, the energy consumption decreases as the specific energy increases (Fig. 11(b)). In this situation, the higher efficiency of the electrical power chain compensates for the power required to fly heavier aircraft.

All three scenarios show a reduction in fuel consumption when $e_{battery}$ is above 400Wh/kg. Specifically, the scenario with the highest battery pack life (Fig. 11(c)) has a constant reduction of fuel consumption (around 2%), except for the battery pack of 750Wh/kg. At the same time, the take-off mass goes down, as fewer batteries are used to compensate for the reduction in effective energy density, aside from when the energy density is high enough to completely compensate for the degradation of the cells.

There is a clear discontinuity in overall behaviour for the high energy density pack and the other low energy density ones, indicating a possible technological tipping point. Indeed, for the low energy densities (as pointed out in Section 5.3) the design takes advantage of the increased specific energy to reduce the number of cells in the battery pack and hence contain the increment of fuel consumption caused by the cells aging and the heavy aircraft. On the contrary, with a battery pack of high specific energy, the margin of fuel consumption reduction is wide enough to accommodate the performance degradation, thus the optimiser is no longer forced to compromise on the size of the battery pack.

Table 6. Details of the selected design points for discussion

$e_{battery}$ (Wh/kg)	Pack life (Days)	r_{degr}	N_{cells}	N_{series}	$N_{modules}$	M_{fuel} (kg)	$M_{battery}$ (kg)	TOM (kg)
450	24	1.0838	44,880	136	663	1,211.2	5,181.8	22,943
500	121	1.0957	46,784	136	344	1,172.6	5,248.1	22,970
550	271	1.1085	112,608	136	828	1,136.9	5,302.5	22,989
750	1,022	1.0009	112,608	136	1,107	983.3	5,199.1	22,990
450	48	1.0299	32,096	136	236	1,228.7	1,839.8	19,618
500	158	1.0197	21,080	136	155	1,225.7	1,085.2	18,860
550	310	1.0168	18,224	136	134	1,222.9	851.9	18,624
750	1071	1.0003	112,608	136	826	1,056.3	3,879.3	21,485

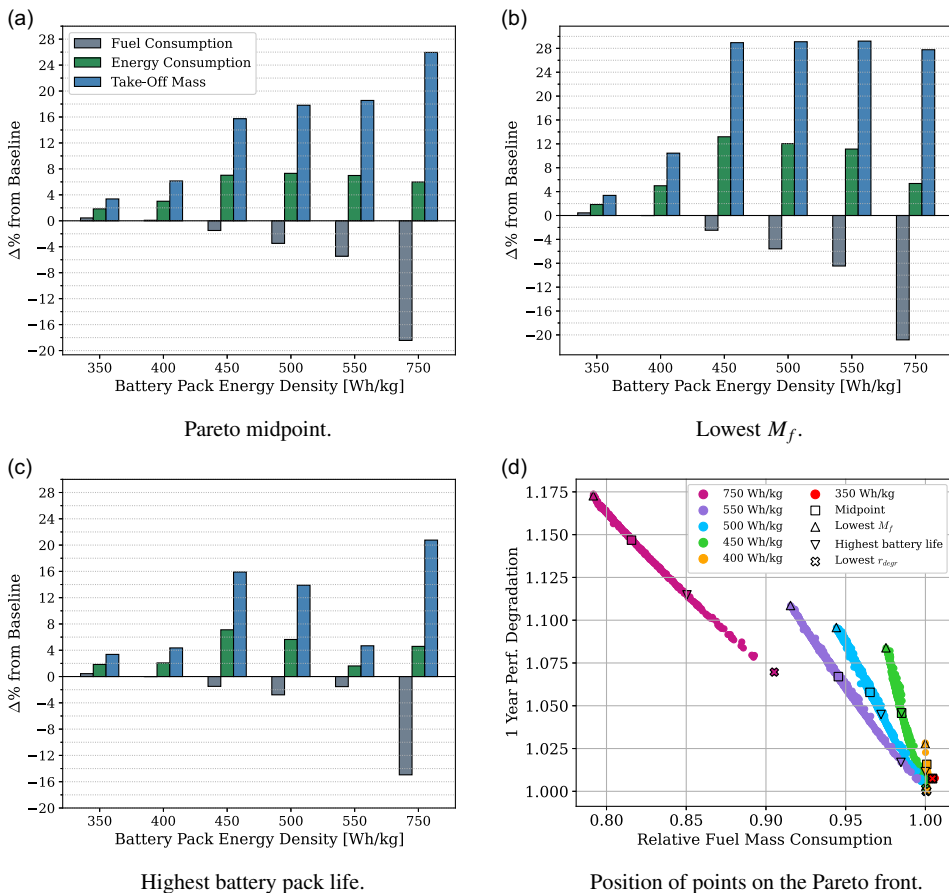


Figure 11. Aircraft performance at representative points in the Pareto front.

It should be noted that the highest battery life points do not correspond to the lowest r_{degr} . Minimising only that objective would entail for most designs, not including any battery pack at all. The fuel consumption would stay identical as the object causing its increment is missing (see Fig. 13(d)).

In general, the Pareto midpoint balances the two extreme cases, with an increase in energy consumption between 7–7.5%. The three scenarios show that when the battery technology is fixed, the choice

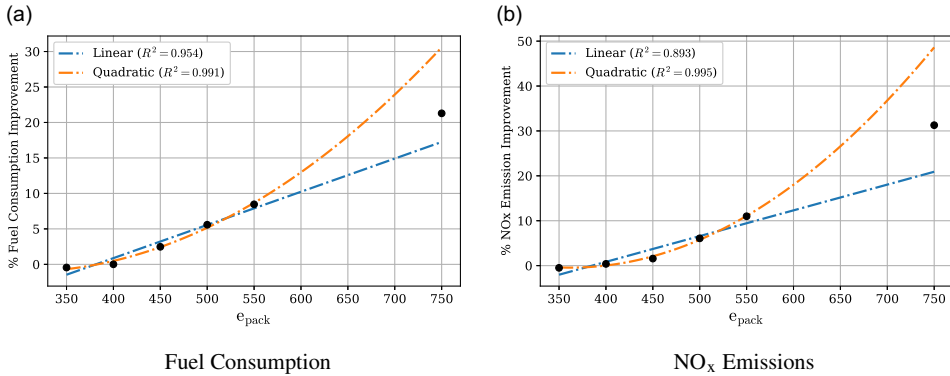


Figure 12. Effects of e_{battery} on performance objectives.

of EMS affects the efficiency of the aircraft, via the increase in battery pack mass. Finally, as cells age, more fuel will be required, increasing the inefficiency in energy consumption.

A final point is to investigate the increment of performance with the increase of e_{battery} . Previous results already suggested a non-linear trend. Figure 12 shows the best-observed improvement for each value of the pack energy density. Two trend lines, one linear and one quadratic, were fitted to the original data set (350–550 Wh/kg) of the previous study [55]. The rate of improvement is non-linear but sub-quadratic, as the new data point falls between the two lines. The nonlinearity stems from the ability of the optimiser to use more electrical energy, which is more efficient and cleaner than fuel, with less weight penalty. Therefore, investing in the improvement of battery technology would have significant returns. This aspect will be explored in the discussion of the technological availability of Section 5.6.

5.5 Suggested energy management strategies

From the knowledge obtained in the previous sections, it was found that the average value of DOH for each segment is correlated with the energy density of the battery and the amount of maximum take-off mass. More DOH is allocated in the climb segment than in the cruise segment, while the slope increases in the cruise and is ambiguous for the climb. Because in this study the battery pack is sized to match the EMS at day zero, the average value of DOH drives the increment of fuel consumption as the battery ages through the mechanism explained in Section 5.3.

Figure 13 presents the EMS of the three scenarios analysed in the previous section plus the EMS with the least r_{degr} . They present the trends described so far, which show no clear preference for the slope of the DOH function in the climb. Higher e_{battery} allows for higher average DOH throughout the mission when fuel consumption is the priority (Fig. 13(b)). In contrast, when battery life is maximised, the higher energy density is used to reduce the amount of battery mass through a reduction of DOH (Fig. 13(c)). As pointed out previously, this condition does not correspond to the EMS of minimum degradation. Instead, the minimum r_{degr} is obtained when no hybridisation is used (Fig. 13(d)). Although in practice this is an undesirable result, it further exhibits the relation between the battery mass and the increment of fuel consumption as the battery pack ages: no increment is present if no batteries are used.

In summary, the presented EMS should be used as a general recommendation considering the identified interactions between pack energy density, battery aging, and environmental requirements. They are limited by the selected design mission, the aircraft design selected as the starting point, and the merit figures selected for the analysis. Consequently, designers should perform their optimisation study for their specific application and use the presented results as a sanity check.

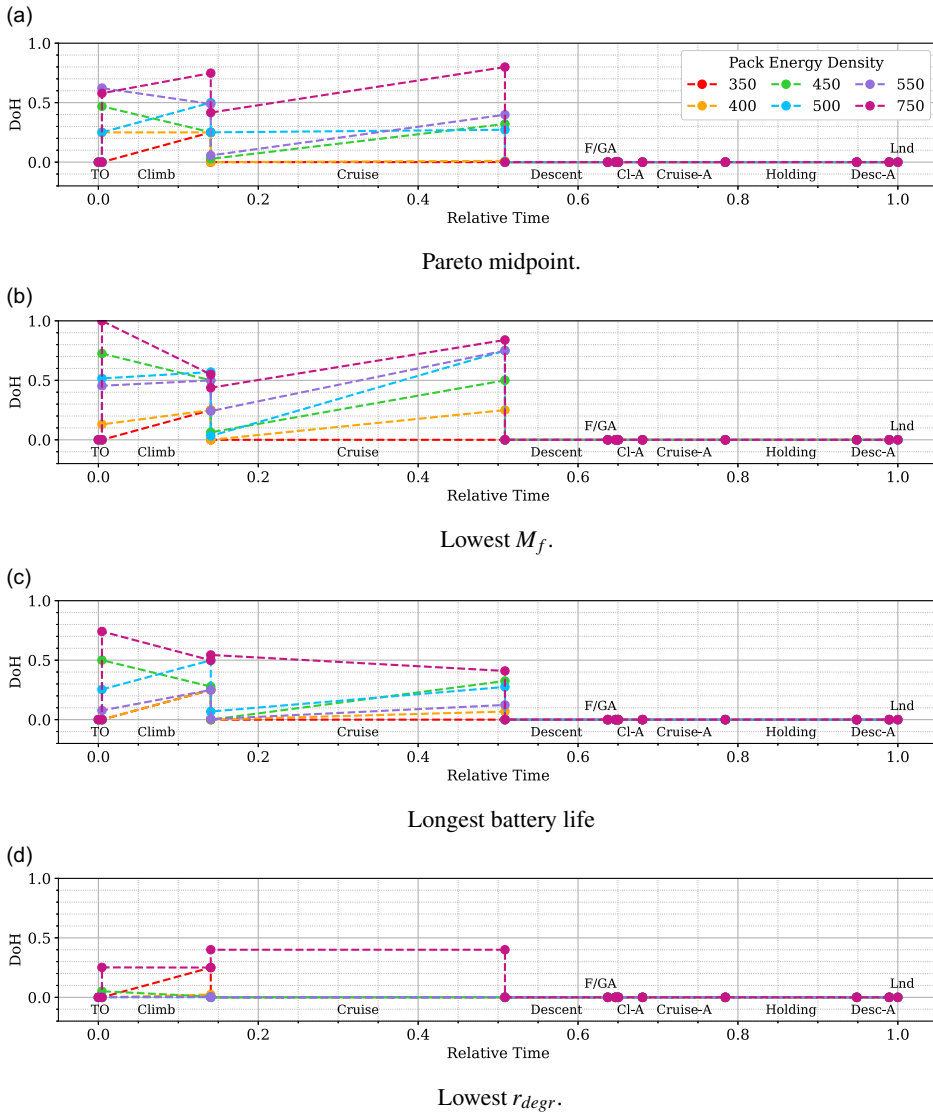


Figure 13. EMS of the three scenarios analysed in Section 5.4, compared to the lowest r_{degr} EMS.

5.6 Probability of achieving the expected technological requirements

The discussion presented so far underlined the importance of $e_{battery}$ for the feasibility of the scenarios presented in this study and hybrid-electric propulsion. However, most studies do not quantify the uncertainty of their timelines; instead, they assume a year far in the future to justify their assumption. In this last section, the probability of technological availability is estimated with a regression analysis of current and expected specific cell energy densities. The intention is to quantify when it is reasonable to expect the required values $e_{battery}$ to be given the history of cell technology development.

Data have been extracted from the Battery 2030+ Roadmap report [42] from 2010 onward. Two scenarios are presented, one conservative and one optimistic. The first assumes that the cell energy density will improve linearly over time (Fig. 14(a)). The second scenario assumes that it will improve exponentially (Fig. 14(b)). Ordinary Least Squares (OLS) have been used to construct the regression

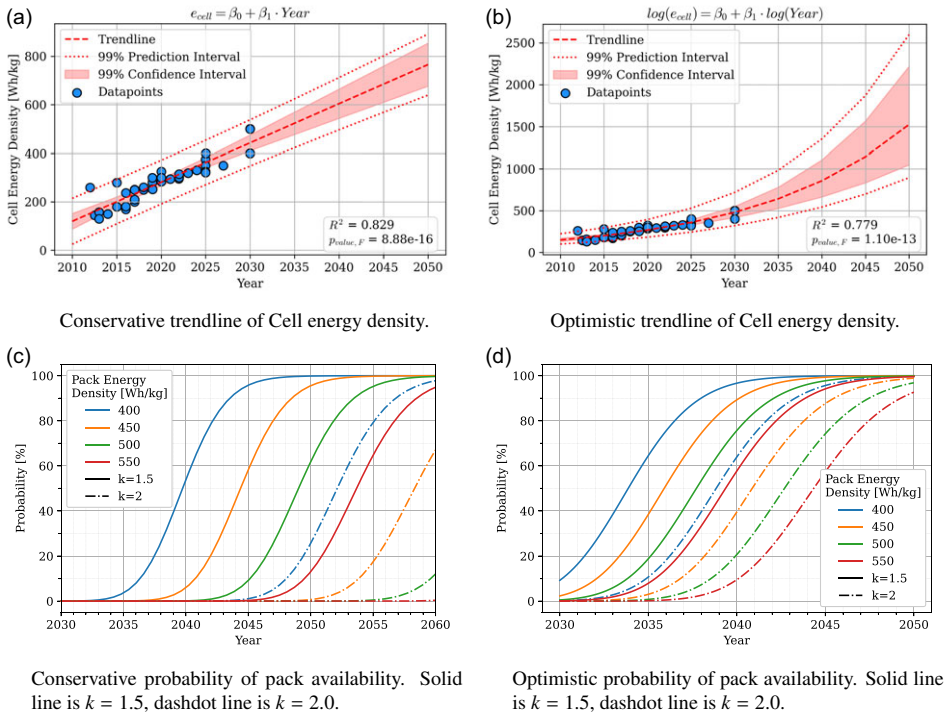


Figure 14. Statistical modeling of future battery technology.

models using standard procedures. Both models have a satisfactory correlation ($R^2 = 0.83$ and $R^2 = 0.78$, respectively) and good modeling (the P values of the F test are lower than 1^{-10} in both cases).

The energy density of battery packs is lower than that of cell packs because of the inert mass added by the cooling system, packaging, and control electronics. Two values of the pack-to-cell ratio, 1.5 and 2.0, have been used to evaluate the impact of this technological uncertainty on the final pack energy density. Figure 14(c) and (d) present these results for the values of $e_{battery}$, which could match or improve on the baseline.

The two scenarios are considerably different, even for the same value of k . Under the conservative scenario and $k = 1.5$, 2040 is the earliest date at which a 400Wh/kg battery pack is expected to be available with 55% confidence. On the contrary, the optimistic scenario estimates the year 2034 for the same value and confidence. This difference is more pronounced for higher energy densities. In the conservative scenario, in 2050 there is a 60% chance that a battery pack with 500Wh/kg is available, while in the optimistic scenario, the year 2038 is indicated. For a very high value of 750Wh/kg, the availability is predicted far in the future, with the earliest date being 2045 on the most optimistic conditions. This value of energy density might be achievable earlier with other technologies, for instance, fuel cells driven by PowerPaste [57].

Furthermore, the assumed pack-to-cell ratio significantly affects the predicted availability. In the conservative scenario, the technological gap is on average 15 years, up to 18 years for the highest value of energy density. This reduces to five years if the optimistic scenario is assumed. The full range of predictions is presented in Table 7.

As noted above, this analysis leads to different conclusions on the feasibility of hybrid-electric aircraft. While the conservative scenario is the most likely, the automotive and renewable sectors have been heavily investing in the development of the technology, which could accelerate the rate of development.

Table 7. Predicted years of e_{battery} technological availability

	k	Conservative				Optimistic			
		1.5		2.0		1.5		2.0	
		50%	90%	50%	90%	50%	90%	50%	90%
e_b (Wh/kg)	400	2,039	2,043	2,052	2,057	2,034	2,038	2,039	2,043
	450	2,044	2,048	2,058	2,063	2,036	2,040	2,041	2,045
	500	2,049	2,053	2,064	2,070	2,037	2,042	2,043	2,047
	550	2,053	2,058	2,071	2,077	2,039	2,044	2,044	2,049
	750	2,072	2,079	2,096	2,105	2,045	2,050	2,049	2,055

Indeed, the comparison shown in Fig. 12 suggests the potential for significant performance improvement, which is shown to be nonlinear, hence targeting the development of cells with higher energy density would have a better return on investment.

Furthermore, availability is affected by the packaging factor k , which cannot yet be accurately predicted, as it is affected by both material technology and the safety requirements in the battery pack. However, most of the technological timeframes proposed in Table 1 are unrealistically optimistic unless a significant breakthrough in storage technology materialises.

6.0 Conclusions

In this work, the interaction between battery energy density and energy management strategy on battery pack aging, fuel consumption and environmental compatibility was analysed. The application of a probabilistic design space exploration framework generated data that shed light on the optimal power schedule and the minimal technological requirements.

The specific energy of the batteries was identified as a key driver in the achievable reduction of fuel consumption and emissions, setting the maximum achievable amount of DOH in the EMS. This parameter affects the life of the battery pack, increasing its effective use before the fuel consumption of the airplane is identical to the baseline. Fuel consumption and NO_x emissions were found to improve with increasing specific energy at an increasing rate. This suggests that investing in energy storage technology would yield better returns rather than gradual improvement. Achieving a pack energy density above 550Wh/kg would strongly mitigate the performance degradation due to battery aging, further indicating the need for investment in this technological improvement.

Finally, 400Wh/kg was identified as the minimum specific energy required to improve baseline emissions. This translates into a requirement of cells with 600Wh/kg specific energy, expected to be available between the years 2034–2040, depending on the technological scenario. Battery packs with higher specific energy, required to make hybrid-electric propulsion feasible, are predicted to be available in the 2038–2050 time window. However, this prediction is conditioned by the current trend of technological improvement and a fixed 1.5 pack-to-cell mass weight ratio. Higher values of pack-to-cell mass ratios would shift this scenario further in the future up to 15 years. This coefficient relates to the safety, and potentially there is a trade-off between energy density, durability and safety. In addition, for such technology to become a solution in the real world then aspects of scalability and industrialisation should be considered.

The inclusion of cell aging in the battery model introduced additional considerations in the definition of EMS. While striving for the highest DOH possible is beneficial for the immediate reduction of emissions, it shortens the operational life of the battery pack. The mechanism of this phenomenon was identified not in the rate of aging of the cells, which was identical in every case studied, but in the number of batteries employed in each specific case. In fact, as the batteries aged, the effective energy density of the pack decreased, requiring the aircraft to consume more fuel. This effect is stronger with a heavier

battery pack. Therefore, when trying to minimise the effects of degradation, the optimiser identified the designs with the least number of cells, taking advantage of the higher energy density when possible. As a result, EMS should be moderated to avoid quickly degrading zero-day performance.

The knowledge obtained in this study is limited to a single mission. Introducing different operating missions would provide more insight into the trade-off between battery ageing and reducing fuel consumption and emissions. This would be of interest to airline operators employing hybrid-electric aircraft, minimising direct operating costs and programming maintenance, for instance, by matching battery pack and gas turbine maintenance schedules.

Another possible extension is to introduce operating conditions that would directly affect cell aging. The scenario presented in this paper assumed full discharge and recharge of the battery pack after each flight. However, partial recharging and discharging are necessary for high-volume operations and fast turnaround of the aircraft [56]. This would introduce stresses that would directly affect the health of cells. Finally, the assumption of constant cell temperature could be relaxed with the introduction of a seasonal effect or a thermal management system cooling model [58].

Finally, the insights obtained in this study requires further validation as the model used did not take into account the cell chemistry and the impact of new energetic materials. These would affect the ageing modelling and the timeline prediction. However, the reader should appreciate the difficulty in this task and the level of multi-disciplinary expertise required to model and predict these trends in a credible way. As discussed in Section 2.0, many studies of hybrid-electric aircraft completely ignore this aspect and prefer to select arbitrarily a year and pack energy density. It is of interest of the aeronautical community and stakeholders to have realistic assumptions and realistic goals, as the current climate emergency calls for immediate and rapid intervention for introducing sustainable and net-zero technologies.

Acknowledgements. This project has received funding from the European Union's Horizon 2020 Research and Innovation programme under Grant Agreement No 875551. Dr Spinelli extends his gratitude to Dr Bahareh Zaghari and Tianzhi Zhou for their contributions to the development of the battery pack model. He acknowledges Dr. Evangelia Pontika for her assistance with mission analysis modeling and Dr. Hossein B. Enalou for his expertise in the gas turbine model. Additionally, he thanks Anthony Roubinet from Institut Polytechnique de Grenoble for providing additional test case data.

References

- [1] Bowman, C.L., Felder, J.L. and Marien, T.V. Turbo-and hybrid-electrified aircraft propulsion concepts for commercial transport, 2018 AIAA/IEEE Electric Aircraft Technologies Symposium (EATS), 2018, p 4984.
- [2] Xie, Y., Savvaris, A., Tsourdos, A., Zhang, D. and Gu, J. Review of hybrid electric powered aircraft, its conceptual design and energy management methodologies, *Chin. J. Aeronaut.*, 2021, **34**, (4), pp 432–450.
- [3] Riboldi, C.E.D. Energy-optimal off-design power management for hybrid-electric aircraft, *Aerospace Sci. Technol.*, 2019, **95**, p 105507.
- [4] Pinto Leite, J.P.S. and Voskuijl, M. Optimal energy management for hybrid-electric aircraft, *Aircraft Eng. Aerospace Technol.*, 2020, **92**, (6), pp. 851–861.
- [5] Spinelli, A., Enalou, H.B., Zaghari, B., Kipouros, T. and Laskaridis, P. Application of Probabilistic set-based design exploration on the energy management of a hybrid-electric aircraft, *Aerospace*, 2022, **9**, (3), p 147.
- [6] Sahoo, S., Zhao, X., Kyprianidis, K.G. and Kalfas, A. Performance assessment of an integrated parallel hybrid-electric propulsion system aircraft, Turbo Expo: Power for Land, Sea, and Air, 2019, vol. 3, doi: [10.1115/GT2019-91459](https://doi.org/10.1115/GT2019-91459)
- [7] Gesell, H., Wolters, F. and Plohr, M. System analysis of turbo-electric and hybrid-electric propulsion systems on a regional aircraft, *Aeronaut. J.*, 2019, **123**, pp 1602–1617.
- [8] Trainelli, L. and Perkon, I. MAHEPA—A Milestone-Setting Project in Hybrid-Electric Aircraft Technology Development, *MEA2019-More Electric Aircraft*, 2019.
- [9] Antcliff, K.R., Guynn, M.D., Marien, T., Wells, D.P., Schneider, S.J. and Tong, M.J. Mission analysis and aircraft sizing of a hybrid-electric regional aircraft, 54th AIAA Aerospace Sciences Meeting, 2016, p 1028.
- [10] Bradley, M.K. and Droney, C.K. Subsonic Ultra Green Aircraft Research: Phase II—volume II—hybrid electric design exploration, *NASA CR-218704*, 2015, NASA.
- [11] Zamboni, J., Vos, R., Emeneth, M. and Schneegans, A. A method for the conceptual design of hybrid electric aircraft, AIAA Scitech 2019 Forum, 2019, p 1587.
- [12] Voskuijl, M., Van Bogaert, J. and Rao, A.G. Analysis and design of hybrid electric regional turboprop aircraft, *CEAS Aeronaut. J.*, 2018, **9**, pp 15–25.

- [13] Strack, M., Chiozzotto, G.P., Iwanizki, M., Plohr, M. and Kuhn, M. Conceptual design assessment of advanced hybrid electric turboprop aircraft configurations, 17th AIAA Aviation Technology, Integration, and Operations Conference, 2017, p 3068.
- [14] Hoelzen, J., Liu, Y., Bensmann, B., Winnefeld, C., Elham, A., Friedrichs, J. and Hanke-Rauschenbach, R., Conceptual design of operation strategies for hybrid electric aircraft, *Energies*, 2018, **11**, p 217.
- [15] Spierling, T. and Lents, C. Parallel hybrid propulsion system for a regional turboprop: conceptual design and benefits analysis, 2019 AIAA/IEEE Electric Aircraft Technologies Symposium (EATS), 2019, pp 1–7.
- [16] Janek, J. and Zeier, W.G. A solid future for battery development, *Nat. Energy*, 2016, **1**, pp 1–4.
- [17] Chin, J.C., Look, K., McNichols, E.O., Hall, D.L., Gray, J.S. and Schnulo, S.L. Battery cell-to-pack scaling trends for electric aircraft, 2021 AIAA/IEEE Electric Aircraft Technologies Symposium (EATS), 2021, pp 1–15.
- [18] Eisenhut, D., Moebis, N., Windels, E., Bergmann, D., Geiß, I., Reis, R. and Strohmayr, A. Aircraft requirements for sustainable regional aviation, *Aerospace*, 2021, **8**, (3), p 61.
- [19] Orifice, F., Nicolosi, F., Corcione, S. and Della Vecchia, P. Hybridization and mission analysis of a regional turboprop, AIAA Aviation 2021 Forum, 2021, p 2421.
- [20] Decerio, D.P. and Hall, D.K. Benefits of parallel hybrid electric propulsion for transport aircraft, *IEEE Trans. Transp. Electrif.*, 2022, **8**, pp 4054–4066.
- [21] Pastra, C.L., Dull, C., Berumen, R., Yumuk, C., Cinar, G. and Mavris, D.N. Viability study of an electrified regional turboprop, 2022 IEEE Transportation Electrification Conference & Expo (ITEC), 2022, pp 231–236.
- [22] Cinar, G., Cai, Y., Bendarkar, M.V., Burrell, A.I., Denney, R.K. and Mavris, D.N. System analysis and design space exploration of regional aircraft with electrified powertrains, *J. Aircraft*, 2023, **60**, pp 382–409.
- [23] Marien, T.V., Blaesser, N.J., Frederick, Z.J., Guynn, M.D., Kirk, J.T., Fisher, K., Schneider, S., Thacker, R.P. and Frederic, P. Results for an electrified aircraft propulsion design exploration, 2021 AIAA/IEEE Electric Aircraft Technologies Symposium (EATS), 2021, pp 1–16.
- [24] Clarke, M. and Alonso, J.J. Lithium-ion battery modeling for aerospace applications, *J. Aircraft*, 2021, **58**, pp 1323–1335.
- [25] Clarke, M.A. and Alonso, J.J. Forecasting the operational lifetime of battery-powered electric aircraft, *J. Aircraft*, 2023, **60**, (1), pp 47–55.
- [26] Donato, T. and Ficarella, A. A modeling approach for the effect of battery aging on the performance of a hybrid electric rotorcraft for urban air-mobility, *Aerospace*, 2020, **7**, (5), p 56.
- [27] Pomet, C., Gologan, C., Vratny, P.C., Seitz, A., Schmitz, O., Isikveren, A.T. and Hornung, M. Methodology for sizing and performance assessment of hybrid energy aircraft, *J. Aircraft*, 2015, **52**, pp 341–352.
- [28] Riboldi, C.E.D. An optimal approach to the preliminary design of small hybrid-electric aircraft, *Aerospace Sci. Technol.*, 2018, **81**, pp 14–31.
- [29] Sahoo, S., Zhao, X. and Kyprianidis, K. A review of concepts, benefits, and challenges for future electrical propulsion-based aircraft, *Aerospace*, 2020, **7**, (4), p 44.
- [30] Brelje, B.J. and Martins, J.R.R.A. Electric, hybrid, and turboelectric fixed-wing aircraft: A review of concepts, models, and design approaches, *Progr. Aerospace Sci.*, 2019, **104**, pp 1–19.
- [31] Liu, X., Furrer, D., Kusters, J. and Holmes, J. Vision 2040: A Roadmap for Integrated, Multiscale Modeling and Simulation of Materials and Systems, *NASA/CR–2018-219771*, 2018.
- [32] Bianchi, D., Amadori, K., Bäckström, E., Jouannet, C. and Secco, N. An uncertainty-based framework for technology portfolio selection for future aircraft program, AIAA Scitech 2021 Forum, 2021, p 1479.
- [33] Guenov, M.D., Chen, X., Molina-Cristóbal, A., Riaz, A., van Heerden, A.S.J. and Padulo, M. Margin allocation and tradeoff in complex systems design and optimization, *AIAA J.*, 2018, **56**, pp 2887–2902.
- [34] Wahler, N.F., Maruyama, D. and Elham, A. Credibility-based multidisciplinary design optimisation of electric aircraft, AIAA SCITECH 2023 Forum, 2023, p 1847.
- [35] Spinelli, A. and Kipouros, T. PDOPT: A Python library for Probabilistic Design space exploration and OPTimisation, *J. Open Source Software*, 2024, **9**, (95), p 6110.
- [36] Spinelli, A., Anderson, L., Enalou, H.B., Zaghari, B., Kipouros, T. and Laskaridis, P. Application of Probabilistic principles to Set-Based Design for the optimisation of a hybrid-electric propulsion system, *IOP Conf. Ser. Mater. Sci. Eng.*, 2022, **1226**, (1), p 012064.
- [37] Singer, D.J., Doerry, N. and Buckley, M.E. What is set-based design?, *Naval Eng. J.*, 2009, **121**, pp 31–43.
- [38] Costa, R. and Sobek, D.K. Iteration in engineering design: Inherent and unavoidable or product of choices made?, International Design Engineering Technical and Computers and Information in Engineering Conference, vol. 37017, 2003, pp 669–674.
- [39] McKenney, T.A., Kemink, L.F. and Singer, D.J. Adapting to changes in design requirements using set-based design, *Naval Eng. J.*, 2011, **123**, (3), pp 67–77.
- [40] Parsons, M.G., Singer, D.J. and Sauter, J.A. A hybrid agent approach for set-based conceptual ship design, 10th International Conference on Computer Applications in Shipbuilding (ICCAS), 1999, pp 207–221.
- [41] Kipouros, T., Inselberg, A., Parks, G. and Savill, A.M. Parallel coordinates in computational engineering design, 54th AIAA/ASME/ASCE/AHS/ASC Structures, Structural Dynamics, and Materials Conference, 2013, p 1750.
- [42] Edstrom, K., Ayerbe, E., Cekic-Laskovic, I., Dominko, R., Fichtner, M., Grimaud, A. and Vegge, T. Battery 2030+: Inventing the sustainable batteries of the future. Research Needs and Future Actions. BATTERY 2030+ Roadmap. Retrieved from https://battery2030.eu/wp-content/uploads/2022/07/BATTERY-2030-Roadmap_Revision_FINAL.pdf, 2022.
- [43] Chin, J., Schnulo, S.L., Miller, T., Prokopius, K. and Gray, J.S. Battery performance modeling on SCEPTOR X-57 subject to thermal and transient considerations, AIAA Scitech 2019 Forum, 2019.

- [44] ATR ATR-72-600 Factsheet. Retrieved from https://www.atr-aircraft.com/wp-content/uploads/2020/07/Factsheets_-_ATR_72-600.pdf, 2022.
- [45] Jackson, P., Peacock, L., Bushell, S., Willis, D. and Winchester, J. Jane's All the Worlds Aircraft: Development and Production 2018-2019, IHS Markit, 2018.
- [46] MacMillan, W.L. Development of a Modular-Type Computer Program for the Calculation of Gas Turbine Off-Design Performance, PhD thesis, Cranfield University, Cranfield UK, 1974.
- [47] Nkoi, B., Pilidis, P. and Nikolaidis, T. Performance of small-scale aero-derivative industrial gas turbines derived from helicopter engines, *Propul. Power Res.*, 2013, **2**, (4), pp 243–253.
- [48] DuBois, D. and Paynter, G.C. "Fuel Flow Method2" for estimating aircraft emissions, SAE International Non-Conference Specific Technical Papers, 2006.
- [49] Filipponi, A. and Bojdo, N. Statistical model for gas turbine engines exhaust emissions, *Transp. Res. Part D Transp. Environ.*, 2018, **59**, pp 451–463.
- [50] Cano, T.C., Castro, I., Rodriguez, A., Lamar, D.G., Khalil, Y.F., Albiol-Tendillo, L. and Kshirsagar, P. Future of electrical aircraft energy power systems: An architecture review, *IEEE Trans. Transp. Electrification*, 2021, **7**, pp 1915–1929.
- [51] Chen, M. and Rincon-Mora, G.A. Accurate electrical battery model capable of predicting runtime and I-V performance, *IEEE Trans. Energy Convers.*, 2006, **21**, (2), pp 504–511.
- [52] Ceraolo, M., Lutzemberger, G. and Huria, T. Experimentally-determined models for high-power lithium batteries, SAE 2011 World Congress & Exhibition, 2011, p 1365.
- [53] Schmalstieg, J., Käbitz, S., Ecker, M. and Sauer, D.U. A holistic aging model for Li(NiMnCo)O₂ based 18650 lithium-ion batteries, *J. Power Sources*, 2014, **257**, pp 325–334.
- [54] Moebs, N., Eisenhut, D., Windels, E., van der Pols, J. and Strohmayer, A. Adaptive initial sizing method and safety assessment for hybrid-electric regional aircraft, *Aerospace*, 2022, **9**, p 3.
- [55] Spinelli, A., Krupa, G.P. and Kipouros, T. Set-based design space exploration to investigate the effect of energy storage durability on the energy management strategy of a hybrid-electric aircraft, AIAA SCITECH 2023 Forum, 2023, p 0837.
- [56] Spinelli, A., Krupa, G.P., Kipouros, T., Berseneff, B. and Fiette, S. Investigation of the operational flexibility of a regional hybrid-electric aircraft, *J. Phys. Conf. Ser.*, 2023, **2526**, (1), p 012021.
- [57] Heubner, F. and Vogt, M. Powerpaste in Aviation: Powerpaste for aviation energy supplies, Fraunhofer IFAM, 2023, Fraunhofer Institute for Manufacturing Technology and Advanced Materials IFAM Branch Lab Dresden.
- [58] Gkoutzamanis, V.G., Tsentis, S.E., Valsamis Mylonas, O.S., Kalfas, A.I., Kyprianidis, K.G., Tsirikoglou, P. and Sielemann, M. Thermal management system considerations for a hybrid-electric commuter aircraft, *J. Thermophys. Heat Transfer*, 2022, **36**, pp 650–666.